PHYSICAL REVIEW B **93**, 201108(R) (2016)

# Many-electron expansion: A density functional hierarchy for strongly correlated systems

Tianyu Zhu, Piotr de Silva, Helen van Aggelen, and Troy Van Voorhis*

*Department of Chemistry, Massachusetts Institute of Technology, 77 Massachusetts Avenue, Cambridge, Massachusetts 02139, USA*

(Received 11 August 2015; revised manuscript received 11 April 2016; published 19 May 2016)

Density functional theory (DFT) is the *de facto* method for the electronic structure of weakly correlated systems. But for strongly correlated materials, common density functional approximations break down. Here, we derive a many-electron expansion (MEE) in DFT that accounts for successive one-, two-, three-, ... particle interactions within the system. To compute the correction terms, the density is first decomposed into a sum of localized, nodeless one-electron densities ($\rho_i$). These one-electron densities are used to construct relevant two- ($\rho_i + \rho_j$), three- ($\rho_i + \rho_j + \rho_k$), ... electron densities. Numerically exact results for these few-particle densities can then be used to correct an approximate density functional via any of several many-body expansions. We show that the resulting hierarchy gives accurate results for several important model systems: the Hubbard and Peierls-Hubbard models in 1D and the pure Hubbard model in 2D. We further show that the method is numerically convergent for strongly correlated systems: applying successively higher order corrections leads to systematic improvement of the results. MEE thus provides a hierarchy of density functional approximations that applies to both weakly and strongly correlated systems.

DOI: 10.1103/PhysRevB.93.201108

The promise of density functional theory (DFT) is tantalizing: there exists a single universal functional, $F[\rho]$, that predicts the electronic ground state of all molecules and materials exactly [1–3]. Unfortunately, while this functional is universal in principle, in practice one encounters an ever-growing list of specific functionals that have been tailored to particular physical conditions [4–6]. The proliferation of functionals is in part due to the difficulty of accounting for strong correlation (sometimes called static correlation) within DFT. Commonly used approximate functionals deal well with weak correlation, but to varying degrees fail for strong correlation, where a different set of approximations must be employed [7–11]. In this Rapid Communication, we bridge this gap by deriving a hierarchy of density functional approximations that systematically correct for strong correlation in a numerically accessible form.

We begin by recognizing that strong correlation is typically short-ranged. This physics is, for example, at the heart of dynamical mean field theory [12]. To account for this in DFT, assume that we can decompose the total spin density $[\rho(\mathbf{r},\sigma)]$ into a sum of localized one-electron spin densities $[\rho_i(\mathbf{r},\sigma)]$:

$$\rho(\mathbf{r},\sigma) \equiv \sum_{i=1}^{N} \rho_i(\mathbf{r},\sigma), \qquad \int \rho_i(\mathbf{r},\sigma) d\mathbf{r} = 1. \tag{1}$$

We will further stipulate that each $\rho_i(\mathbf{r},\sigma)$ should be ground-state $v$-representable [13]. Next, suppose we can compute the energy of the entire system with some approximate density functional $E_a[\rho]$ while we can obtain the exact energy $E_v[\rho]$ only for a few electrons at once. For any $\rho$, define $\Delta E[\rho] \equiv E_v[\rho] - E_a[\rho]$ and consider the following hierarchy of approximations:

$$\begin{aligned}
E_0[\rho] &\equiv E_a[\rho], \\
E_1[\{\rho_i\}] &\equiv E_0[\rho] + \sum_{i}^{N} \Delta E[\rho_i], \\
E_2[\{\rho_i\}] &\equiv E_1[\{\rho_i\}] + \sum_{i<j}^{N} (\Delta E[\rho_i + \rho_j] - \Delta E[\rho_i] \\
&\quad - \Delta E[\rho_j]), \\
E_3[\{\rho_i\}] &\equiv E_2[\{\rho_i\}] + \sum_{i<j<k}^{N} (\Delta E[\rho_i + \rho_j + \rho_k] \\
&\quad - \Delta E[\rho_i + \rho_j] - \Delta E[\rho_j + \rho_k] \\
&\quad - \Delta E[\rho_i + \rho_k] + \Delta E[\rho_i] + \Delta E[\rho_j] \\
&\quad + \Delta E[\rho_k]), \\
&\cdots .
\end{aligned} \tag{2}$$

Equation (2) is the central result of this Rapid Communication. Note that $E[\rho]$ means the total energy, but one could replace $E[\rho]$ with the universal functional $F[\rho]$ or with the sum of Hartree and exchange-correlation energies $E_{\mathrm{Hxc}}[\rho]$, which would fit Eq. (2) into the Kohn-Sham framework. This many-electron expansion (MEE) is closely related to the many-body expansion for intermolecular interactions [14,15] and the method of increments [16]. MEE has the important property that $E_i[\rho]$ gives the exact energy for $i$ electrons no matter what approximate functional $E_a$ is chosen. It thus provides a hierarchy of approximations within the context of DFT analogous to many-body theory [17] for the Green's function and the coupled-cluster expansion of the wave function [18].

For spin-compensated systems, it makes sense to decompose the total density rather than the spin density. In this case, one naturally obtains *pair* densities

$$\rho(\mathbf{r}) \equiv \sum_{i=1}^{N/2} \rho_i(\mathbf{r}), \qquad \int \rho_i(\mathbf{r}) d\mathbf{r} = 2. \tag{3}$$

We will call the analogous expansion to Eq. (2) using $\rho_i(\mathbf{r})$ the many-pair expansion (MPE). For MPE, $E_i$ is exact for $2i$ electrons and only requires calculations on spin-compensated densities, which simplifies the intermediate calculations.

*tvan@mit.edu

 

In order to compute the MEE or MPE energies, we need the approximate and exact ground-state energies for various fragment densities $\rho_q$, noting that these fragment densities will typically only involve a few electrons. Assuming the approximate energy derives from Kohn-Sham DFT (KS-DFT), $E_a[\rho_q]$ is easily obtained via potential inversion techniques [19–21]. One invents a noninteracting reference determinant, $\Phi$, constructed out of orbitals $\phi_k(\mathbf{r})$. One then searches for the stationary point of the Lagrangian

$$L_{KS}[\phi_k, v_s] \equiv \langle\Phi| - \frac{1}{2}\nabla^2|\Phi\rangle + \int v_s(\mathbf{r})\left[\sum_k |\phi_k(\mathbf{r})|^2 - \rho_q(\mathbf{r})\right]d\mathbf{r}. \quad (4)$$

Functionally, this optimization is done sequentially. For a given $v_s$ each KS orbital satisfies a one-electron Schrödinger equation:

$$-\tfrac{1}{2}\nabla^2\phi_k(\mathbf{r}) + v_s^q(\mathbf{r})\phi_k(\mathbf{r}) = \epsilon_k\phi_k(\mathbf{r}). \quad (5)$$

One then solves for $v_s^q$ which gives the desired density $\rho_q$ and $E_a[\rho_q] \equiv E_a[\{\phi_k\}]$ where any implicit orbital dependence in the functional is now explicit in terms of the optimized KS orbitals.

To obtain $E_v[\rho_q]$, one can perform a similar potential inversion construction for the interacting system [22]. One invents an interacting state $|\Psi\rangle$ and searches for the stationary point of

$$L_{\text{Exact}}[\Psi, v_{ex}] \equiv \langle\Psi|\left[\frac{1}{2}\sum_k \hat{\mathbf{p}}_k^2 + \sum_{k<l}\frac{1}{\hat{r}_{kl}}\right]|\Psi\rangle + \int v_{\text{ex}}(\mathbf{r})[\langle\Psi|\delta(\hat{\mathbf{r}} - \mathbf{r})|\Psi\rangle - \rho_q(\mathbf{r})]d\mathbf{r}. \quad (6)$$

The result is the ground state of the *fully interacting* system with a potential $v_{\text{ex}}^q(\mathbf{r})$:

$$\left[\frac{1}{2}\sum_k \hat{\mathbf{p}}_k^2 + \sum_{k<l}\frac{1}{\hat{r}_{kl}} + v_{\text{ex}}^q(\hat{\mathbf{r}})\right]|\Psi\rangle = E|\Psi\rangle, \quad (7)$$

where $v_{\text{ex}}^q$ is chosen such that $\langle\Psi|\delta(\hat{\mathbf{r}} - \mathbf{r})|\Psi\rangle = \rho_q(\mathbf{r})$ and the final energy is given by $E_v[\rho_q] \equiv \langle\Psi|\hat{H}|\Psi\rangle$. At this point it becomes clear why the fragment densities must be $v$-representable: in order for there to be some interacting system that gives the right fragment density, the density itself must be the ground state of *some* potential.

Because the MEE$n$ (MPE$n$) energy $E_n[\rho]$ is an approximation to the *variational* functional $E_v[\rho]$, we can also use $E_n[\rho]$ to approximate the interacting ground-state density. The variationally optimal density $\rho_0$ is the one that satisfies

$$\left.\frac{\delta E_n[\rho]}{\delta\rho}\right|_{\rho_0} = \mu, \quad (8)$$

where $\mu$ is the global chemical potential. This results in a one-electron Schrödinger equation for the MEE$n$- or MPE$n$-KS orbitals

$$-\tfrac{1}{2}\nabla^2\phi_k(\mathbf{r}) + v_n(\mathbf{r})\phi_k(\mathbf{r}) = \epsilon_k\phi_k(\mathbf{r}), \quad (9)$$

where the effective potential for each level in the hierarchy includes contributions from the $n$th-order energy corrections:

$$v_1(\mathbf{r}) = v_s(\mathbf{r}) + \sum_i \int \left(\frac{\delta E_v[\rho]}{\delta\rho_i(\mathbf{r}')} - \frac{\delta E_a[\rho]}{\delta\rho_i(\mathbf{r}')}\right)\frac{\delta\rho_i(\mathbf{r}')}{\delta\rho(\mathbf{r})}d\mathbf{r}'$$

$$= v_s(\mathbf{r}) + \sum_i \int [v_{\text{ex}}^i(\mathbf{r}') - v_s^i(\mathbf{r}')]\frac{\delta\rho_i(\mathbf{r}')}{\delta\rho(\mathbf{r})}d\mathbf{r}' \quad (10)$$

$$\equiv v_s(\mathbf{r}) + \delta v_1(\mathbf{r}), \quad (11)$$

$$v_2(\mathbf{r}) = v_1(\mathbf{r}) + \sum_{i<j}\int [v_{\text{ex}}^{ij}(\mathbf{r}') - v_s^{ij}(\mathbf{r}')]\left(\frac{\delta\rho_i(\mathbf{r}')}{\delta\rho(\mathbf{r})} + \frac{\delta\rho_j(\mathbf{r}')}{\delta\rho(\mathbf{r})}\right)d\mathbf{r}' - (N-1)\delta v_1(\mathbf{r}), \quad \cdots. \quad (12)$$

It is thus clear that MEE$n$ (or MPE$n$) also provides a convergent hierarchy of approximations to the true KS potential: beginning with an approximate $v_s$, each $v_n$ provides an improved potential that eventually converges (not necessarily monotonically) to the exact result when $n$ is equal to the total number of electrons (or electron pairs). Note that in order to apply MEE (or MPE), one needs a prescription for obtaining (pair) densities from the total density. One anticipates that different choices for $\rho_i$ could be useful in different scenarios. Thus, we consider the above to be a complete derivation of the MEE$n$ (and MPE$n$) formalism with the understanding that a particular ansatz for $\rho_i$ must be made in practice.

The MEE$n$ hierarchy can also be thought of as a generalization of the Perdew-Zunger self-interaction correction (PZ-SIC) [23]. For $E_{\text{Hxc}}$, MEE1 calculated with orbital densities is equivalent to PZ-SIC; however, such densities are not admissible in MEE as they are not $v$-representable. In both cases, one-electron densities are not defined uniquely. However, whereas PZ-SIC corrects one-electron self-interaction errors [24], MEE$n$ is capable of removing many-electron self-interaction to arbitrary order. In many situations self-interaction mimics correlation in DFT, so that removing self-interaction without adding correlation can make the results worse [25]. In this light, it is important to note that at each order, MPE$n$ compensates for the excluded many-electron self-interaction by including a corresponding degree of many-electron correlation. Thus, MPE$n$ is in some sense balanced, even at low orders.

To illustrate the performance of MEE, we first consider the one-dimensional Hubbard model [26] described by the Hamiltonian

$$\hat{H} = \sum_{i\sigma} t_i(\hat{a}_{i,\sigma}^\dagger\hat{a}_{i+1,\sigma} + \hat{a}_{i+1,\sigma}^\dagger\hat{a}_{i,\sigma}) + U\sum_i \hat{a}_{i,\alpha}^\dagger\hat{a}_{i,\alpha}\hat{a}_{i,\beta}^\dagger\hat{a}_{i,\beta}, \quad (13)$$

where $t_i \equiv t$. The first term describes hopping of electrons between neighboring sites and the second describes on-site repulsion of opposite-spin electrons. The model describes potentially strongly correlated electrons on a lattice and often serves as a benchmark for electronic structure methods [27,28] as the exact solution, based on the Bethe ansatz, is known [29]. Different formulations of DFT exist for the Hubbard model, which differ by the choice of the basic variable in lieu of real-space density [30–32]. In this work, the density of the

system is understood as the diagonal of the density matrix in the site basis. Since the model has translational symmetry under periodic boundary conditions (PBCs), the ground-state density is equal at each site and amounts to $\rho_\alpha = \frac{2N_{\rm occ}}{N}, \forall\alpha = 1,\ldots,N$, where $N_{\rm occ}$ is the number of electron pairs distributed over $N$ sites of the lattice.

As the total ground-state density is known, we can decompose it into a sum of pair densities [Eq. (3)], in principle, by any prescription that assures $v$-representability. One of the necessary conditions for a density to be $v$-representable on a lattice with PBCs is that it be positive at each site [33]. Here, we relax this restriction, requiring only that $\rho_i$ be non-negative, which is feasible if we also allow infinite $v_i$. In practice, we want to partition total density in such a way that pair densities are compact. Physically, this would allow us to interpret them as localized electron pairs and to capture most of the correlation. A viable procedure to achieve such decomposition is to recall the Boys orbital localization criterion [34], which minimizes the spatial spread of orbitals. Applying this procedure to the Hubbard model results in pair densities composed of contiguous blocks (Fig. 1). All numerical results presented in this Rapid Communication are based on this prescription.

For a typical filling, the localization results in pair densities that are inhomogeneous: they equal $N_{\rm occ}/N$ for the central site(s) but only contain part of the density on the edge sites [see Fig. 1(a)]. In this case, the MPE1 correction is a sum of many slightly different energies:

$$E_1[\rho] = E_0[\rho] + \Delta E[\rho_1] + \Delta E[\rho_2] + \Delta E[\rho_3] + \cdots . \tag{14}$$

However, for certain fillings (such as 1/2 or 1/3), the partitioning procedure leads to pair densities that repeat periodically along the chain [see Fig. 1(b)], resulting in an energy $E_1[\rho] = E_0[\rho] + N_{\rm occ}\Delta E[\rho_1]$. Note that this transition happens abruptly; starting from a periodic filling and adding even one electron pair results in a completely aperiodic filling. As a result, the MPE$n$ energy is not a smooth function of filling. A way to resolve this is to average energies over different possible pair density partitions. In practice, we perform the averaging by adding an additional constraint on $\rho_{1,1} = \gamma$ and integrating over $\gamma \in (0, \langle n\rangle]$:

$$E_{AMPE}[\rho] = \int_0^{\langle n\rangle} E_{MPE}(\gamma)d\gamma. \tag{15}$$

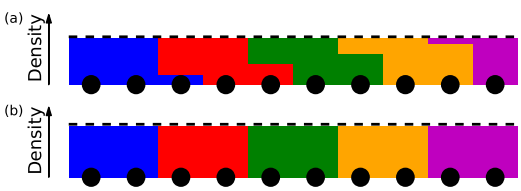


FIG. 1. Localized pair densities for 1D Hubbard model at (a) nonperiodic filling ($\langle n\rangle = 0.9$), (b) periodic filling ($\langle n\rangle = 1.0$). Lattice sites are represented by black circles, while each pair density is marked by one color. The black dashed line is the total density for each site. Note that the pair density picture is incomplete in (a) because the remainder of the lattice is truncated.

We evaluate this integral by quadrature, which then directly mimics the average that is done for the aperiodic filling case [Eq. (14)].

As the approximate functional in Eq. (2), we use the exact exchange (EXX) and local density approximation (LDA). The latter is constructed by fitting the exchange-correlation energy per site to the Bethe ansatz energies. Exact diagonalization is used to compute $E_v[\rho]$. To compute EXX (LDA) and exact energies for the fragment density $\rho_q$, we need to search for the potentials $v_s^q$ and $v_{\rm ex}^q$ in Eq. (5) and Eq. (7). Our numerical algorithm for this is described in the Supplemental Material [39].

In Fig. 2, we plot the averaged MPE (AMPE) energy curve of a 500-site 1D Hubbard model as a function of the site occupancy $\langle n\rangle$. We perform MPE calculations up to the 4th order [Eq. (2)], which means we only need to do exact calculations on up to 4 electron pairs at a time. Thanks to the locality of interactions (A)MPE at any level scales linearly with the system size as opposed to factorial scaling of exact diagonalization. The exact Bethe ansatz (BA) results are presented for comparison. Overall, the AMPE energy curves are in excellent agreement with the BA curve. Even at 1st order, EXX-AMPE is in good agreement with the reference, whereas LDA-AMPE deviates more significantly. Considering that, by design, LDA is exact for the homogeneous Hubbard model, the poor performance of LDA-AMPE1 teaches us something about LDA: while it is exact for the uniform system, treatment of two- and many-electron interactions is unbalanced. Adding in the correct interactions for each pair then makes the results worse because the many-electron errors are exposed and only summation up to the $N$-pair contribution makes the resulting errors cancel. Starting from the 2nd order, curves representing EXX-AMPE and LDA-AMPE energies become visually indistinguishable and the latter are suppressed in Fig. 2 for clarity. As can be seen, when we apply successive higher order corrections, the AMPE energies converge quickly towards the exact result, which confirms that our method can be systematically improved. For reference, the MPE$n$ energies are visually indistinguishable from the AMPE$n$ energies, except

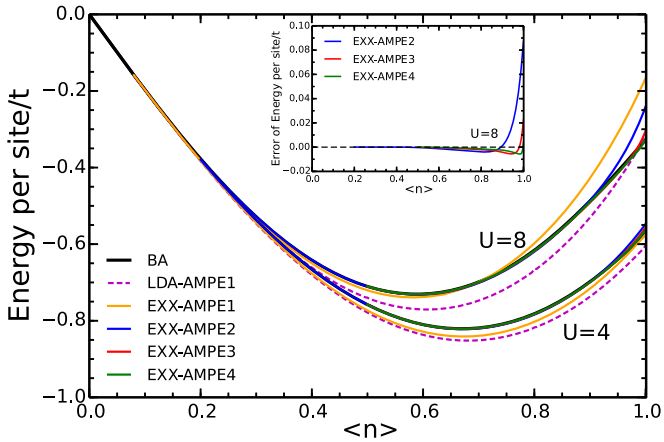


FIG. 2. Energy per site and its errors for 1D Hubbard model as a function of site occupancy $\langle n\rangle$.

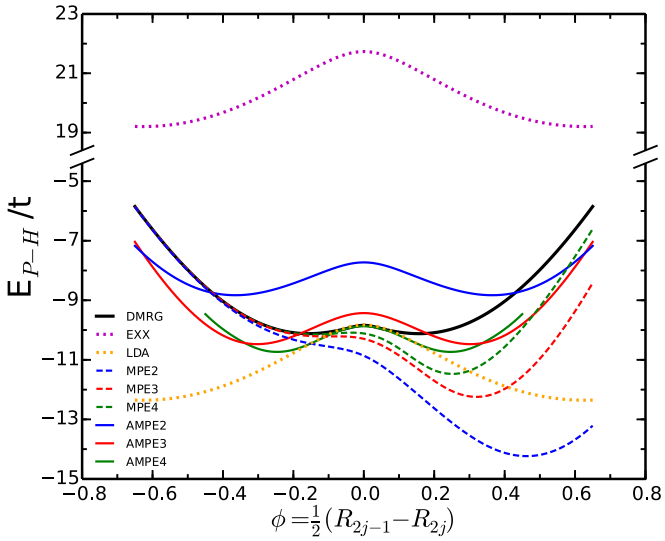


FIG. 3. Energy for 30-site Peierls-Hubbard model as a function of bond shift parameter $\phi$ ($U = 8$, $\langle n \rangle = 1$, $\omega = 2.8t$).

at the periodic fillings, where the MPE$n$ results would be discontinuous.

As the second example, consider the Hubbard model with a Peierls distortion ($t_{2j-1} \neq t_{2j}, j = 1, \ldots, N/2$) [35]. This model reflects the spontaneous symmetry breaking of the 1D periodic lattice resulting, for example, from alternating single and double bonds in a conjugated polymer such as polyacetylene. Such displacement with respect to the symmetric Hubbard model can be described with a bond shift parameter $\phi = \frac{1}{2}(R_{2j-1} - R_{2j})$, where $R_i$ denotes the bond length between sites $i$ and $i+1$. The Hamiltonian takes the form of Eq. (13) with $t_{2j-1} = te^{-\phi}$ and $t_{2j} = te^{\phi}$. Keeping the analogy with polyacetylene, we recognize that the Peierls-Hubbard model only treats the $\pi$ electrons. To incorporate the additional energy cost of stretching and squeezing the underlying $\sigma$ bonds, for a given displacement $\phi$ we add a harmonic term $N\frac{\omega}{2}\phi^2$ to the total energy, where $\omega = 2.8t$ gives approximately the correct physics for $U = 8$. We restrict our model to 30 sites, in which case numerically exact results are easily obtained from DMRG [36,37]. As can be seen in Fig. 3, the exact curve has a symmetric double-well shape characteristic of the expected symmetry breaking. EXX results reproduce this qualitative feature, but are far too high in energy and the predicted bond shifts are too large. LDA results in a uniform downward shift with respect to EXX such that the LDA energy is correct for $\phi = 0$. For $\phi \neq 0$, LDA predicts energies which are far too low, which is again a manifestation of many-electron self-interaction errors in LDA.

At half filling, the Peierls-Hubbard model presents an interesting challenge for MPE. Assuming partitioning into nonoverlapping pair densities [Fig. 1(b)], EXX-MPE and LDA-MPE are equivalent as the LDA correction is exactly canceled out at the 1st order . Averaging leads only to a uniform shift; therefore, only EXX-(A)MPE is explicitly considered in Fig. 3 and in the following discussion. The pair densities [Fig. 1(b)] naturally break the symmetry of the lattice when $\phi \neq 0$: the pairs either localize on a $2j-1,2j$ bond or on a $2j,2j+1$ bond. In the former case, for $\phi < 0$ ($t_{2j-1} > t_{2j}$), the short double bonds are located between two sites occupied by the same density pair; MPE therefore will give a better description than for $\phi > 0$, where the short double bonds are located between different density pairs. This is clearly demonstrated in Fig. 3, where the $2j-1,2j$ is chosen, leading to a very accurate treatment for negative $\phi$, but strong overcorrelation for positive $\phi$. Particularly at high orders, MPE$n$ does an impressive job of reproducing the energy dispersion about the minimum, but the global behavior is unsatisfactory.

To recover the symmetric shape, we again apply the averaging procedure for MPE. By averaging over different pair density partitions, AMPE results do not rely on particular pair density positions. Thus, AMPE avoids MPE's asymmetry problem and finds two local minima correctly. The AMPE$n$ minima clearly approach the DMRG ones as $n$ increases. Nevertheless the convergence to the exact result is rather slow. On the other hand, when $\phi < 0$, MPE is more accurate than AMPE, which suggests that some *a priori* knowledge of the electronic structure could perhaps be used to improve the results: an ansatz capable of picking out the "best" density pattern might be able to capture MPE's accuracy near the minimum together with AMPE's global symmetry.

Finally, we note that MPE is not in any way restricted to 1D systems. For instance, we apply MPE for the 2D Hubbard model, whose sites form a two-dimensional square lattice. Due to the macroscopic degeneracy of the model, there are many equivalent density partitionings making it difficult to arrive at definitive MPE$n$ numbers for the model. Still, for example at $U = 4$ with an $8 \times 8$ lattice the EXX-MPE$n$ error relative to the best estimates [38] goes from 23% to 7.8% to 1.5% as $n$ goes from 1 to 3. More details can be found in the Supplemental Material [39], but this result clearly demonstrates the applicability of MPE to higher dimensional systems.

In this Rapid Communication we have shown that MPE is a systematically improvable hierarchy of density functional approximations to the total energy of a quantum many-body system. The strength of the method is that even at low levels of expansion it can address the problem of strongly correlated electrons in DFT. This has been shown on model lattice Hamiltonians, which capture the essential physics of the problem. As the next step, we are working on implementation of the method for *ab initio* Hamiltonians in order to extend calculations to realistic molecules and solids. Given the elegance of the basic idea, we hope that the discoveries made here will translate easily to these more sophisticated problems.

We thank M. Welborn for Bethe ansatz reference values and Prof. S. Zhang for 2D Hubbard model data. This work was funded by a grant from the NSF (CHE-1464804). T.V. acknowledges support from a David and Lucile Packard Foundation Fellowship.

[1] W. Kohn, Rev. Mod. Phys. **71**, 1253 (1999).
[2] K. Burke, J. Chem. Phys. **136**, 150901 (2012).
[3] A. D. Becke, J. Chem. Phys. **140**, 18A301 (2014).
[4] B. J. Lynch, P. L. Fast, M. Harris, and D. G. Truhlar, J. Phys. Chem. A **104**, 4811 (2000).
[5] Y. Zhao and D. G. Truhlar, Theor. Chem. Acc. **120**, 215 (2008).
[6] J. P. Perdew, A. Ruzsinszky, G. I. Csonka, O. A. Vydrov, G. E. Scuseria, L. A. Constantin, X. Zhou, and K. Burke, Phys. Rev. Lett. **100**, 136406 (2008).
[7] V. I. Anisimov, J. Zaanen, and O. K. Andersen, Phys. Rev. B **44**, 943 (1991).
[8] A. Teale, S. Coriani, and T. Helgaker, J. Chem. Phys. **132**, 164115 (2010).
[9] F. Malet and P. Gori-Giorgi, Phys. Rev. Lett. **109**, 246402 (2012).
[10] J. P. Bergfield, Z.-F. Liu, K. Burke, and C. A. Stafford, Phys. Rev. Lett. **108**, 066801 (2012).
[11] E. M. Stoudenmire, L. O. Wagner, S. R. White, and K. Burke, Phys. Rev. Lett. **109**, 056402 (2012).
[12] W. Metzner and D. Vollhardt, Phys. Rev. Lett. **62**, 324 (1989).
[13] E. H. Lieb, in *Inequalities* (Springer, 2002), pp. 269–303.
[14] J. Cui, H. Liu, and K. D. Jordan, J. Phys. Chem. B **110**, 18872 (2006).
[15] R. M. Richard and J. M. Herbert, J. Chem. Phys. **137**, 064113 (2012).
[16] H. Stoll, J. Chem. Phys. **97**, 8449 (1992).
[17] L. Hedin, Phys. Rev. **139**, A796 (1965).
[18] J. Čížek, J. Chem. Phys. **45**, 4256 (1966).
[19] Q. Zhao, R. C. Morrison, and R. G. Parr, Phys. Rev. A **50**, 2138 (1994).
[20] Q. Wu and W. Yang, J. Chem. Phys. **118**, 2498 (2003).
[21] R. van Leeuwen and E. Baerends, Phys. Rev. A **49**, 2421 (1994).
[22] L. O. Wagner, T. E. Baker, E. M. Stoudenmire, K. Burke, and S. R. White, Phys. Rev. B **90**, 045109 (2014).
[23] J. P. Perdew and A. Zunger, Phys. Rev. B **23**, 5048 (1981).
[24] O. A. Vydrov, G. E. Scuseria, J. P. Perdew, A. Ruzsinszky, and G. I. Csonka, J. Chem. Phys. **124**, 094108 (2006).
[25] O. A. Vydrov and G. E. Scuseria, J. Chem. Phys. **121**, 8187 (2004).
[26] J. Hubbard, Proc. R. Soc. London, Ser. A **276**, 238 (1963).
[27] G. Knizia and G. K.-L. Chan, Phys. Rev. Lett. **109**, 186404 (2012).
[28] K. Boguslawski, P. Tecmer, P. W. Ayers, P. Bultinck, S. De Baerdemacker, and D. Van Neck, Phys. Rev. B **89**, 201106 (2014).
[29] E. H. Lieb and F. Wu, Physica A **321**, 1 (2003).
[30] O. Gunnarsson and K. Schönhammer, Phys. Rev. Lett. **56**, 1968 (1986).
[31] A. Schindlmayr and R. W. Godby, Phys. Rev. B **51**, 10427 (1995).
[32] R. López-Sandoval and G. M. Pastor, Phys. Rev. B **61**, 1764 (2000).
[33] W. Kohn, Phys. Rev. Lett. **51**, 1596 (1983).
[34] S. F. Boys, Rev. Mod. Phys. **32**, 296 (1960).
[35] R. E. Peierls, *Quantum Theory of Solids* (Oxford University Press, Oxford, 1955).
[36] S. R. White, Phys. Rev. Lett. **69**, 2863 (1992).
[37] G. K.-L. Chan and M. Head-Gordon, J. Chem. Phys. **116**, 4462 (2002).
[38] C.-C. Chang and S. Zhang, Phys. Rev. B **78**, 165101 (2008).
[39] See Supplemental Material at http://link.aps.org/supplemental/10.1103/PhysRevB.93.201108 for numerical details of the potential inversion, fitted LDA exchange-correlation energies and 2D Hubbard model results.